Generic dynamics of a simple plankton population model with a non-integer exponent of closure

Andrew M. Edwards [a,*], Martin A. Bees [b]

[a] *Biological Oceanography Section, Bedford Institute of Oceanography B240, Dartmouth, Nova Scotia, Canada B2Y 4A2*
[b] *Department of Mathematics and Statistics, University of Surrey, Guildford, Surrey GU2 5XH, UK*

Abstract

Low-dimensional plankton models are used to help understand measurements of plankton in the world's oceans. The full dynamics of these models and the effects of varying the functional forms are not completely understood. Moreover, the effects of small-scale physical influences are only recently becoming apparent. In particular, turbulence may play a pivotal role in the strategies adopted by predators of zooplankton, and thus may alter the so-called closure term, which models predation on zooplankton when the predators themselves are not being explicitly simulated. We investigate the use of a closure term with a non-integer exponent, allowing determination of the dynamics as the closure term varies continuously between the commonly used linear and quadratic forms. We determine which characteristics of the dynamics are generic, in that they occur for any exponent of closure, and which are purely a consequence of the usual integer exponents. A three-way transcritical bifurcation of three steady states is the generic situation, occurring for all except the purely linear closure term. Hopf bifurcations, consequent limit cycles, and chaotic attractors appear to be generic across all exponents of closure. Oscillations, and hence chaos, had been hypothesised to be eliminated with the use of quadratic closure. © 2000 Elsevier Science Ltd. All rights reserved.

1. Introduction

Simple models of plankton populations often consist of three coupled ordinary differential equations, describing the time-dependence of nutrients, phytoplankton and zooplankton in the upper layer of the ocean, e.g. [1–4]. The zooplankton are eaten by higher predators whose population size is not being explicitly simulated. This predation is therefore represented by a so-called 'closure term', which expresses the rate of zooplankton mortality as a function of the zooplankton concentration. The functional form and associated parameter values chosen for this closure term have been found to exert a strong influence upon the dynamics of the entire simulated system [4]. The most common choices of closure term used by modellers are the linear form dZ, e.g. [2,5,6], where Z is the concentration of zooplankton and d is the mortality rate, and the quadratic form dZ^2, e.g. [1,7,8].

Recently there has been much interest in the effect of turbulence on predation, and the consequent selection of feeding strategies employed by the predators [9,10]. In particular, the predator's effective reaction distance (the distance for which it is able to sense and feed on prey) has been found to decrease with the turbulent energy dissipation rate [11]. Also, the predator's tactics may change from ambush feeding (active predation) to filter feeding (passive predation) depending on the environmental and physical conditions. This can be explained by noting that the higher the local shear rates, the greater the chance that prey will be advected through the predator's effective reaction region. This scenario is likely to be as relevant to higher predators as it is to the lowest predatory trophic level.

---

[*] Corresponding author.
E-mail addresses: andy@caligo.bio.dfo.ca (A.M. Edwards), m.bees@surrey.ac.uk (M.A. Bees).

At its simplest, a filter-feeding strategy may be viewed as a constant response to zooplankton numbers (i.e., linear closure), because the fraction of the available zooplankton population that the higher predator consumes will be proportional to its effective reactive volume, or even the size of its mouth. However, for the ambush-feeding strategy the predators are attracted to large concentrations of zooplankton and are less inclined to feed on low concentrations. Typically, this is represented in population models by the quadratic closure term. It is clear that the proportion of predators adopting each of these strategies will vary in a continuous fashion with respect to the turbulent conditions. Therefore, in this paper we consider a simple closure term with a non-integer exponent of closure, thus allowing us to explore the dynamics of the system as the closure term is gradually varied from linear to quadratic. Specifically, we use the form dZ^m, where $1 \leqslant m \leqslant 2$.

Our model is essentially that formulated by Steele and Henderson [1]. The dynamics of the model using the linear ($m = 1$) and quadratic ($m = 2$) closure terms have been investigated previously [12,13], revealing a rich dynamical structure consisting of transcritical, three-way transcritical, fold, Hopf and period-doubling bifurcations, plus homoclinic connections and chaos, some of which were only found for one choice of closure term. Here, we ascertain how the dynamics change when we move continuously from one form into the other (i.e., as m varies from 1 to 2, or from 2 to 1), and thus determine which features are unique to either $m = 1$ or $m = 2$, and which are generic in that they occur for all $1 \leqslant m \leqslant 2$.

We outline the model in Section 2. In Section 3, we summarise previously calculated analytical results concerning steady states and their stability for $m = 1$ and $m = 2$. Then we numerically compute bifurcation diagrams, illustrating the existence of two transcritical bifurcations for $m = 1$, and a 'three-way transcritical bifurcation' (whereby three steady states pass through each other and change stability) for $m = 2$. One might expect the three-way bifurcation to be more structurally unstable to changes in model structure than the two separate transcritical bifurcations that exist for $m = 1$, in the sense that the three-way bifurcation can be viewed as the conjunction of the two transcritical bifurcations, and would thus split into the two transcritical bifurcations when the model structure is perturbed. However, in Section 4 we use $1 < m < 2$, and find the dynamics to be qualitatively the same as for $m = 2$. Hence, the $m = 2$ three-way bifurcation represents the generic case, rather than the $m = 1$ bifurcations.

Oscillations arising from Hopf bifurcations have been examined previously for $m = 1$ and $m = 2$ [12,13]. In Section 5, we show that these are the 'same' bifurcations when the dZ^m closure term is used and m varies from 1 to 2. Unforced oscillations had earlier been eliminated in a simple model by the use of $m = 2$ instead of $m = 1$ [4], and it had been thought that this may translate into a general rule for models. Oscillations are intriguing features of plankton population models that warrant investigation [14], and oscillations and chaos in a simple resource competition model have recently been proposed as a mechanism for sustaining plankton biodiversity [15].

Chaotic trajectories have only previously been found for the linear case in this model [13], but are known to occur [16] when quadratic closure is used in the simple three-species food chain model of Hastings and Powell [17]. Thus, we know that it is not a general rule of simple models that setting $m = 2$ precludes chaos. But, until now, it has not been ascertained if chaos is eliminated from the simple Steele and Henderson [1] plankton model with $m = 2$, due to the differences in model structure (e.g., the presence of recycling terms, the use of alternative functional forms) from the Hastings and Powell model. This prompts us in Section 6 to locate chaotic trajectories for the $1 < m \leqslant 2$ situation. We do find chaos for this range, and as an example we present a chaotic attractor that coexists with a limit cycle for $m = 2$, thus completing the set of basic attractors (steady state, limit cycle and chaotic) calculated for $m = 2$.

As far as we are aware, this work presents the first analytical calculations for the use of a non-integer exponent for zooplankton mortality. Such a theoretical grounding is desirable if the current interest in turbulence-related feeding strategies results in widespread use of such a closure term, or related terms, by modellers.

2. Model structure

We use a three-component model based on that of Steele and Henderson [1], to represent concentrations of nutrient (N), phytoplankton (P) and zooplankton (Z) in a physically homogeneous oceanic mixed layer. Phytoplankton, aquatic plants that are mostly unicellular, take up nutrients from the water in order to

photosynthesise. The phytoplankton are grazed upon by the animal zooplankton, which in turn provide sustenance for the higher trophic levels of the food web. Fig. 1 illustrates the structure of the model, whereby arrows indicate flows of matter through the system, and arrows not starting or not ending at a compartment represent the input to and the losses from the modelled system.

The changes in N, P and Z are given by three coupled ordinary differential equations:

$$\frac{dN}{dt} = -\text{uptake} + \text{respiration} + Z \text{ excretion} + Z \text{ predation excretion} + \text{mixing},$$

$$\frac{dP}{dt} = \text{uptake} - \text{respiration} - \text{grazing by } Z - \text{sinking} - \text{mixing},$$

$$\frac{dZ}{dt} = \text{growth} - \text{higher predation}.$$

When the explicit functional forms are included, the model becomes:

$$\frac{dN}{dt} = -\frac{N}{e+N}\frac{a}{b+cP}P + rP + \frac{\beta\lambda P^2}{\mu^2+P^2}Z + \gamma dZ^m + k(N_0 - N), \tag{1}$$

$$\frac{dP}{dt} = \frac{N}{e+N}\frac{a}{b+cP}P - rP - \frac{\lambda P^2}{\mu^2+P^2}Z - (s+k)P, \tag{2}$$

$$\frac{dZ}{dt} = \frac{\alpha\lambda P^2}{\mu^2+P^2}Z - dZ^m. \tag{3}$$

The parameter definitions are given in Table 1, together with the value of each parameter originally used by Steele and Henderson [1]. The equations of the model are described in detail (for linear and quadratic closure) in [12,13]; here we briefly outline the formulation of the model.

A physically homogeneous mixed layer is assumed, within which volumetric concentrations of N, P and Z are uniform. Units of N, P and Z are g C m^{-3}, with time t measured in days, and all parameters are positive. The ratios to convert back into units of nitrogen or chlorophyll, as used by [1], are 1 g carbon $\equiv$ 20 mg chlorophyll $\equiv$ 10 mmol nitrogen. The mixed-layer depth is kept fixed at 12.5 m, and
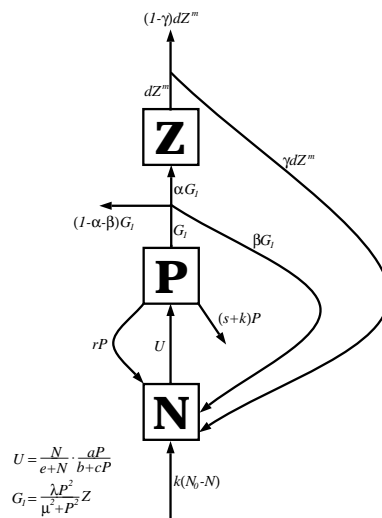

Fig. 1. Interactions between nutrients (N), phytoplankton (P) and zooplankton (Z). Arrows indicate flows of matter through the system, and are labelled with the functions used to model the processes. Open-ended arrows indicate the input to and the losses from the system.

Table 1
Parameter definitions and default values. A range for d is given, since 0.075 was the default value for $m = 1$ used by Edwards and Brindley [13], and 1.0 was the value for $m = 2$ used by Steele and Henderson [1]

Parameter	Symbol	Default value
a/b gives maximum P growth rate	a	$0.2 \text{ m}^{-1} \text{ day}^{-1}$
Light attenuation by water	b	0.2 m^{-1}
P self-shading coefficient	c	$0.4 \text{ m}^2 \text{ (g C)}^{-1}$
Higher predation on Z	d	$0.075 - 1.0 \text{ (g C m}^{-3})^{1-m} \text{ day}^{-1}$
Half-saturation constant for N uptake	e	0.03 g C m^{-3}
Cross-thermocline exchange rate	k	0.05 day^{-1}
Exponent for predation on Z	m	$1 \leqslant m \leqslant 2$
P respiration rate	r	0.15 day^{-1}
P sinking loss rate	s	0.04 day^{-1}
N concentration below mixed layer	N_0	0.6 g C m^{-3}
Z growth efficiency	α	0.25
Z excretion fraction	β	0.33
Regeneration of Z predation excretion	γ	0.5
Maximum Z grazing rate	λ	0.6 day^{-1}
Z grazing half-saturation coefficient	μ	0.035 g C m^{-3}

there is no explicit time-dependence on the right-hand sides of Eqs. (1)–(3), i.e., it is an autonomous dynamical system. The water below the mixed layer is assumed to have zero phytoplankton and zooplankton (and any phytoplankton lost from the mixed layer cannot return to the mixed layer), but a constant nutrient concentration of N_0.

In Fig. 1, the $k(N_0 - N)$ arrow represents the input of nutrients to the system, where k is the exchange rate of water between the mixed layer and the deep water, due to processes such as diffusion and internal-wave breaking. The nutrients decrease due to uptake by phytoplankton. The specific phytoplankton growth rate is limited by nutrient availability, as given by the Michaelis–Menten function $N/(e + N)$ where e is the half-saturation constant, and by available light, the $a/(b + cP)$ term. The maximum daily growth rate averaged over the depth of the mixed layer is given by a/b, where a can be related [18] to the canonical form for primary production derived in [19,20], and b represents the attenuation of irradiance by the water; c is the attenuation by the phytoplankton.

The phytoplankton concentration decreases due to a combined respiration and natural mortality term (r), which is recycled into nutrient, and due to sinking (s) and exchange with the phytoplankton-devoid deep water (k). Phytoplankton are grazed upon by zooplankton as modelled by the Holling type III function $\lambda P^2/(\mu^2 + P^2)$, with maximum grazing rate λ and half-saturation constant μ. The fraction α of this grazing represents the growth efficiency of the zooplankton, and a fraction β represents excretion, which gets regenerated into utilisable nutrient. The remaining fraction $1 - \alpha - \beta$ consists of zooplankton faecal pellets, which are assumed to sink out of the mixed layer immediately.

The zooplankton get eaten by higher predators, whose population is not being explicitly modelled. This process is represented by the closure term, the function dZ^m where $1 \leqslant m \leqslant 2$. The range on m is imposed because for $m < 1$ the per capita mortality rate dZ^{m-1} is unbounded as Z gets small, and $m > 2$ represents an accelerating per-capita rate, which is generally considered biologically unrealistic [16]. A proportion γ of the higher predation is recycled back into N as excretion by the predators, and the remaining $1 - \gamma$ fuels the growth of the predators. Eqs. (1)–(3) are simply obtained from Fig. 1 by summing the inputs and losses for each compartment.

3. Analysis of steady states with $m = 1$ and $m = 2$

The steady states are solutions (N, P, Z) to $dN/dt = dP/dt = dZ/dt = 0$. The steady states and their stability were established in [12,13] for the two separate cases $m = 1$ and $m = 2$. We briefly explain those results (summarised in Table 2) and then compute bifurcation diagrams, in order to set the scene for calculating the behaviour for $1 < m < 2$.

Table 2
The stabilities of the steady states for $m = 1$ and $m = 2$ are determined by Φ and Ω, which are functions of the parameters (defined in the main text)

Steady state	$m = 1$	$m = 2$
$(N_0, 0, 0)$	$\Phi < 0$: stable	$\Phi < 0$: stable
	$\Phi > 0$: unstable	$\Phi > 0$: unstable
$(N_1^*, P_1^*, 0)$	$\Phi < 0$: unrealistic ($P_1^* < 0$)	$\Phi < 0$: unrealistic ($P_1^* < 0$)
	$\Phi > 0$: realistic	$\Phi > 0$: realistic
	stable for $\Omega < 0$	always unstable
	unstable for $\Omega > 0$	
(N^*, P^*, Z^*)	$\Omega < 0$: unrealistic ($Z^* < 0$)	$\Phi < 0$: unrealistic ($P^* < 0$)
	$\Omega > 0$: realistic	$\Phi > 0$: realistic
	stable close to $\Omega = 0$	stable close to $\Phi = 0$
	unique steady state in	multiple steady states possible
	positive octant	in positive octant
	$\Rightarrow$ no fold bifurcations	$\Rightarrow$ fold bifurcations possible

The steady state $(N_0, 0, 0)$ exists for all parameters for both cases, and its stability (Table 2) depends on the sign of Φ, where

$$\Phi = \frac{aN_0}{b(e + N_0)} - r - s - k.$$

There is also a steady state $(N_1^*, P_1^*, 0)$, where N_1^* is the positive root of

$$ckN^2 + \left[\frac{a(s + k)}{r + s + k} - b(s + k) + ck(e - N_0) \right] N - (b(s + k) + ckN_0)e = 0, \tag{4}$$

and P_1^* is given by

$$P_1^* = \frac{k(N_0 - N_1^*)}{s + k}. \tag{5}$$

P_1^* has the same sign as Φ, and as $\Phi \to 0$ we have $P_1^* \to 0$, and $N_1^* \to N_0$, i.e., $(N_1^*, P_1^*, 0) \to (N_0, 0, 0)$. Stability calculations show that there is a transcritical bifurcation for $m = 1$ closure.

For steady states with $Z \neq 0$, which we write as (N^*, P^*, Z^*), setting $dZ/dt = 0$ for $m = 1$ yields an explicit expression for P^*:

$$P^* = \sqrt{\frac{d}{\alpha\lambda - d}} \mu. \tag{6}$$

However, setting $dZ/dt = 0$ for $m = 2$ gives Z as a function of P,

$$Z = \frac{\alpha\lambda P^2}{d(\mu^2 + P^2)}, \tag{7}$$

which then has to be substituted into $dN/dt = 0$ and $dP/dt = 0$. Elimination of N from the two equations leaves P^* as the intractable solution to a tenth-order polynomial.

For $m = 1$, (N^*, P^*, Z^*) exchanges stability with $(N_1^*, P_1^*, 0)$ at a transcritical bifurcation at $\Omega = 0$, where

$$\Omega = \left(N_0 - \frac{(s + k)}{k} P^* \right) \left[\frac{a}{b + cP^*} - (r + s + k) \right] - (r + s + k)e. \tag{8}$$

For $m = 2$, $(N_0, 0, 0)$, $(N_1^*, P_1^*, 0)$ and (N^*, P^*, Z^*) all coincide at a three-way transcritical bifurcation (a term first coined in [21]) at $\Phi = 0$. Close to this bifurcation, for $\Phi < 0$ $(N_0, 0, 0)$ is stable, whereas for $\Phi > 0$ (N^*, P^*, Z^*) is stable; $(N_1^*, P_1^*, 0)$ is always unstable.

In Figs. 2 and 3, we illustrate the nature of these transcritical bifurcations, by numerically computing the steady states and their stabilities as one of the parameters is varied. The three steady states are colour-coded: $(N_0, 0, 0)$ is green, $(N_1^*, P_1^*, 0)$ is purple and (N^*, P^*, Z^*) is red. Solid, dotted and dashed lines are used to indicate the stability of the steady states and the signs of the real parts of the eigenvalues (of the Jacobian at the steady states), as indicated by the key in each figure. Note that the green and purple horizontal lines in Figs. 2(c) and 3(c) are slightly offset from $Z = 0$ for clarity. Figs. 2(d) and 3(d) show how the steady states move about in three-dimensional N–P–Z phase space as r varies; the green point indicates that $(N_0, 0, 0)$ remains in the same location.

All of the parameters are set to the values given in Table 1 and the values and stabilities of the steady states are calculated and portrayed in the figures. The respiration rate, r, is then chosen as the parameter to vary, because it appears in the definitions of Φ and Ω, and at particular values it gives the bifurcations at $\Phi = 0$ and $\Omega = 0$. The default value of r is 0.15, for which $\Phi > 0$ and $\Omega > 0$. For linear closure $d = 0.075$
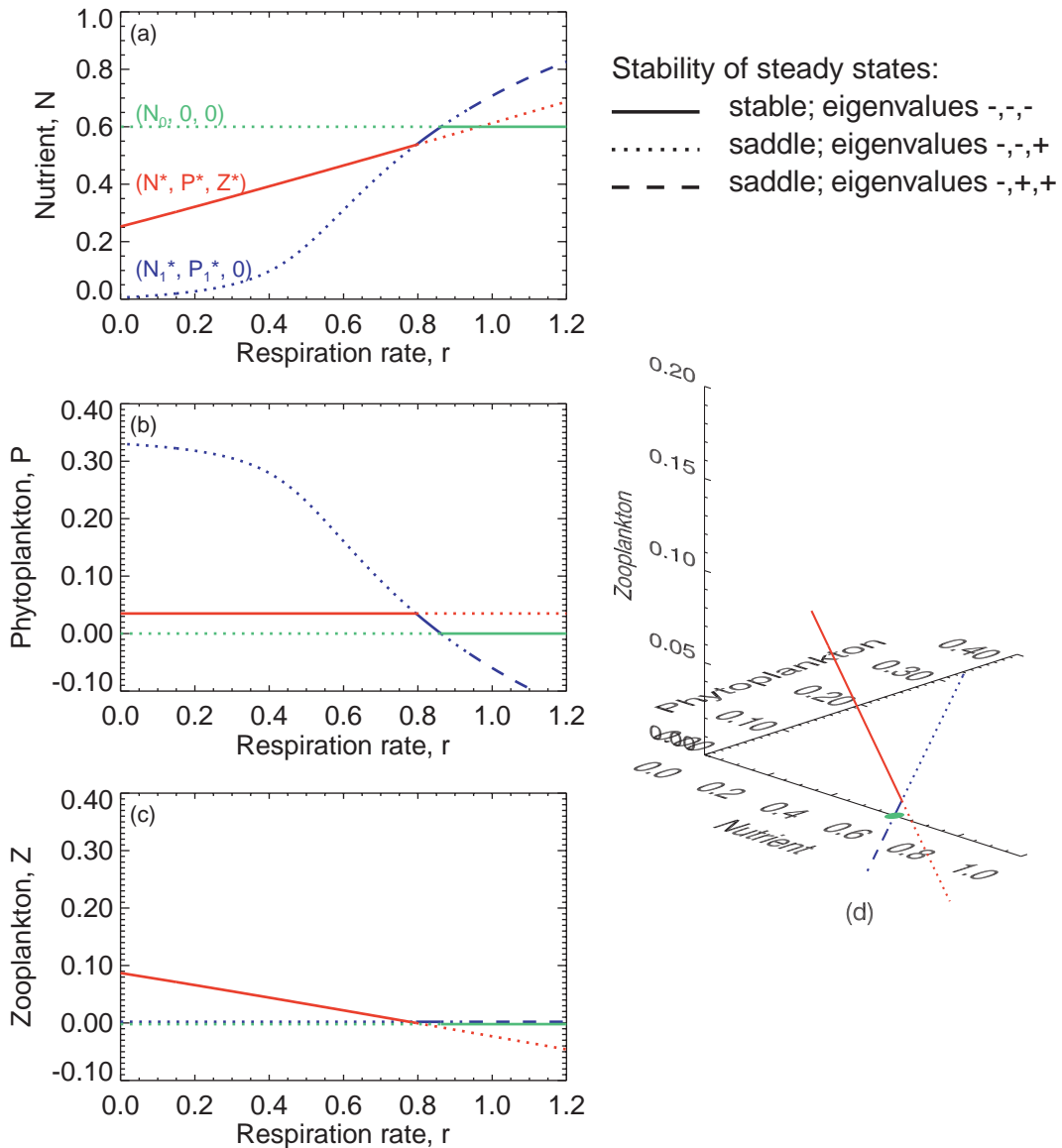

Fig. 2. Location and stability of $(N_0, 0, 0)$, $(N_1^*, P_1^*, 0)$ and (N^*, P^*, Z^*) as r is varied with linear closure ($m = 1$ and $d = 0.075$). The key indicates the signs of the real parts of the eigenvalues and corresponding stabilities of the steady states. Transcritical bifurcations occur at $r = 0.80$ ($\Omega = 0$) and $r = 0.86$ ($\Phi = 0$). Units of N, P and Z are g C m^{-3}, and of r are day^{-1}.
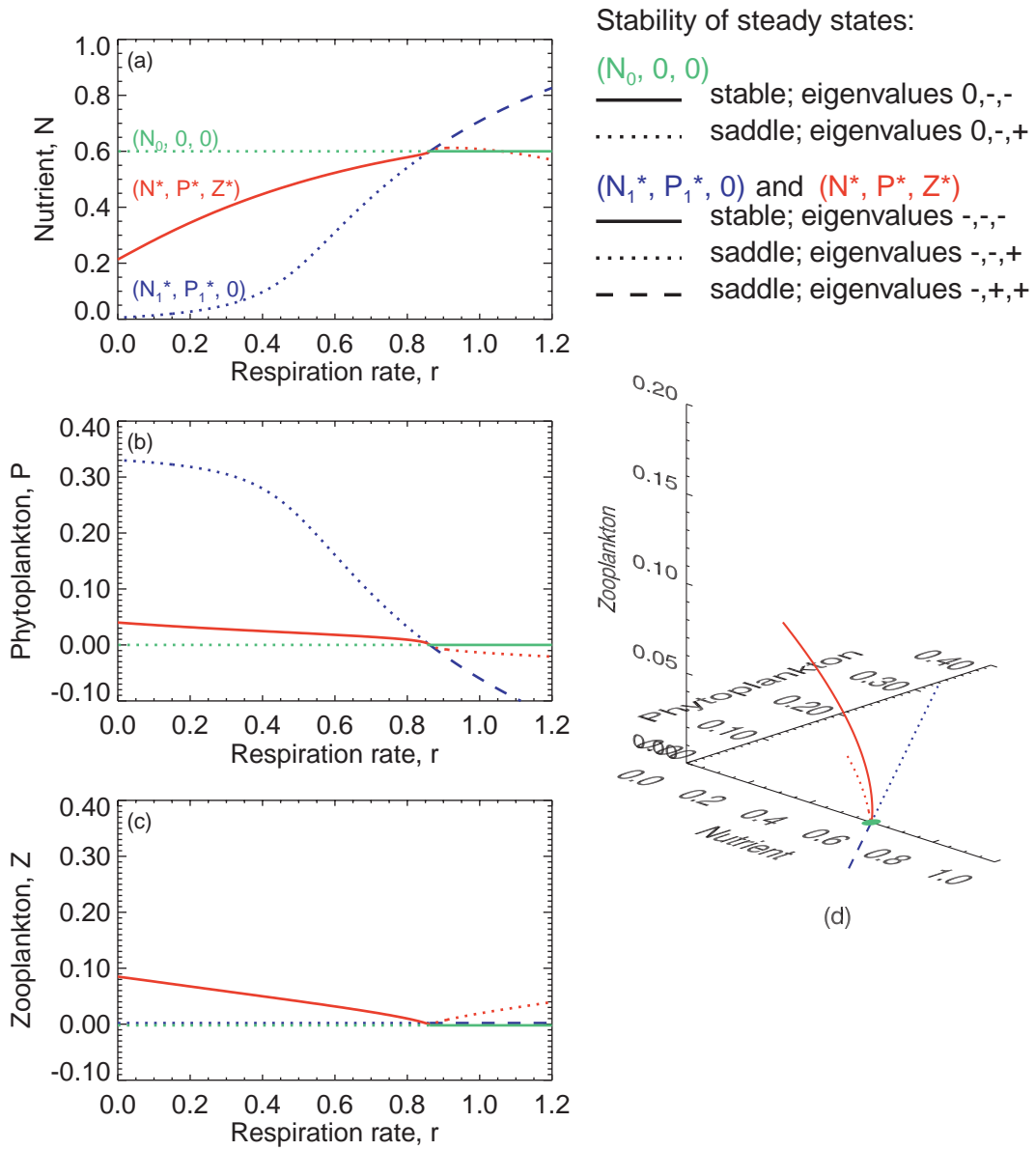
Fig. 3. As for Fig. 2, but with quadratic closure ($m = 2$ and $d = 1$). At $r = 0.86$ ($\Phi = 0$) there is a three-way transcritical bifurcation, whereby all three steady states pass through each other. The two transcritical bifurcations from Fig. 2 occur here at the same point. Units are as in Fig. 2.

and for quadratic closure $d = 1$, in order to minimise quantitative differences in steady-state values between the two closure terms (at least for the default value of r) [13]. The numerical calculations were performed using the bifurcation package LOCBIF [22,23].

In Fig. 2 for linear closure, at low values of r (N^*, P^*, Z^*) is in the positive octant $\{N, P, Z > 0\}$ and is stable (solid red line) because $\Omega > 0$. As r increases, N^* increases, P^* remains constant and Z^* decreases, passing through zero when $r = 0.80$, which is the transcritical bifurcation at $\Omega = 0$. Thus stability is transferred to $(N_1^*, P_1^*, 0)$, the solid purple line, which remains stable until $r = 0.86$, corresponding to $\Phi = 0$. At this point the second transcritical bifurcation occurs, and stability is transferred to $(N_0, 0, 0)$, the solid green line, which remains stable for $r > 0.86$.

For $m = 2$, Fig. 3 shows that (N^*, P^*, Z^*) is stable for values of r up until $r = 0.86$ ($\Phi = 0$). The diagrams show how all three steady states pass through $(N_0, 0, 0) = (0.6, 0, 0)$ at this point, which is the three-way

transcritical bifurcation. As r increases further, $(N_1^*, P_1^*, 0)$ and (N^*, P^*, Z^*) both leave the positive octant (P_1^* and P^* both become negative), and $(N_0, 0, 0)$ is the only ecologically realistic steady state, and is stable.

It appears that the three-way transcritical bifurcation for $m = 2$ may have split into two transcritical bifurcations when $m = 1$, allowing $(N_1^*, P_1^*, 0)$ to have a region of stability. Shortly, we establish which is the more generic behaviour, in terms of what happens for $1 < m < 2$. In both cases (N^*, P^*, Z^*) loses stability as it leaves the positive octant $\{N, P, Z > 0\}$, but this occurs in different ways. For the quadratic case (N^*, P^*, Z^*) passes through the N-axis (for which $P = 0$ and $Z = 0$), whereas for the linear case it passes through the $Z = 0$ plane with $P \neq 0$, as is most clearly seen in the three-dimensional Figs. 3(d) and 2(d), respectively.

Fig. 2(b) shows how the phytoplankton steady-state value P^* remains constant as r varies for $m = 1$, even though r is a direct phytoplankton loss rate. Established in (6), this shows that P^* is independent of all of the parameters which do not appear in the dZ/dt equation, including r and the phytoplankton growth terms. This is a consequence of the linear zooplankton mortality term, and does not occur for the quadratic case.

Note that in Fig. 2, at $r = 0.94$ the eigenvalues of $(N_1^*, P_1^*, 0)$ change from having real parts with signs $-, -, +$ to $-, +, +$ (which implies that they must all be real), as indicated by the purple line changing from dotted to dashed. This is due to $(N_1^*, P_1^*, 0)$ undergoing a third transcritical bifurcation, this time with the steady state (N_-^*, P_-^*, Z_-^*) which arises from using the negative root, P_-^*, of Eq. (6). Since this steady state can never enter the ecologically realistic positive octant its nature was not considered further in the analysis, and for clarity it is not drawn in Fig. 2. Although the range of r considered here is outside the realistic range tabulated in [12], the bifurcations can be reached if the mixed layer deepens, for example, when considering an annual variation in the mixed-layer depth [18].

4. Analysis of steady states with $1 < m < 2$

We now investigate how the dynamics change as m varies continuously between the two cases studied above. This will ascertain whether the behaviour for $1 < m < 2$ matches that for either the $m = 1$ or $m = 2$ case.

The local stability of a steady state is determined by the eigenvalues of the Jacobian matrix, which in this case is given by

$$\mathbf{A} = \begin{bmatrix} -\frac{aeP}{(e+N)^2(b+cP)} - k & -\frac{abN}{(e+N)(b+cP)^2} + r + \frac{2\beta\lambda\mu^2 PZ}{(\mu^2+P^2)^2} & \frac{\beta\lambda P^2}{\mu^2+P^2} + m\gamma dZ^{m-1} \\ \frac{aeP}{(e+N)^2(b+cP)} & \frac{abN}{(e+N)(b+cP)^2} - r - s - k - \frac{2\lambda\mu^2 PZ}{(\mu^2+P^2)^2} & -\frac{\lambda P^2}{\mu^2+P^2} \\ 0 & \frac{2\alpha\lambda\mu^2 PZ}{(\mu^2+P^2)^2} & \frac{\alpha\lambda P^2}{\mu^2+P^2} - md Z^{m-1} \end{bmatrix},$$

evaluated at the steady-state values of N, P and Z. Steady states with $Z = 0$ will have the same definitions as those for the $m = 1, 2$ cases.

The steady state $(N, P, Z) = (N_0, 0, 0)$ exists for all parameter values, and the Jacobian at $(N_0, 0, 0)$ is

$$\mathbf{A} = \begin{bmatrix} -k & -\frac{aN_0}{b(e+N_0)} + r & \begin{cases} \gamma d & (m = 1) \\ 0 & (m > 1) \end{cases} \\ 0 & \Phi & 0 \\ 0 & 0 & \begin{cases} -d & (m = 1) \\ 0 & (m > 1) \end{cases} \end{bmatrix},$$

where { indicates that certain terms depend upon the value of m. The dynamics will not change smoothly as $m \to 1$, since the two terms in the third column are not continuous at $m = 1$. In particular, the (3,3) term is an eigenvalue, and is identically zero for $m > 1$ but non-zero at $m = 1$. Numerical experiments indicate that the stability of $(N_0, 0, 0)$ is the same for $1 < m < 2$ as for $m = 2$, i.e., stable for $\Phi < 0$ and unstable for $\Phi > 0$.

The Jacobian at $(N_1^*, P_1^*, 0)$ is

$$\mathbf{A} = \begin{bmatrix} -\frac{aeP}{(e+N)^2(b+cP)} - k & -\frac{abN}{(e+N)(b+cP)^2} + r & \begin{cases} \frac{\beta\lambda P^2}{\mu^2+P^2}+\gamma d & (m=1) \\[2mm] \frac{\beta\lambda P^2}{\mu^2+P^2} & (m>1) \end{cases} \\[6mm] \frac{aeP}{(e+N)^2(b+cP)} & \frac{abN}{(e+N)(b+cP)^2} - r - s - k & -\frac{\lambda P^2}{\mu^2+P^2} \\[6mm] 0 & 0 & \begin{cases} \frac{\alpha\lambda P^2}{\mu^2+P^2}-d & (m=1) \\[2mm] \frac{\alpha\lambda P^2}{\mu^2+P^2} & (m>1) \end{cases} \end{bmatrix},$$

where $(N, P, Z) = (N_1^*, P_1^*, 0)$. The $(3, 3)$ component determines the stability (the other two eigenvalues are negative), so $(N_1^*, P_1^*, 0)$ is never stable for $m > 1$, but can be for $m = 1$. Thus, for $m > 1$, the zooplankton can never die out (starting from a strictly positive concentration) unless the phytoplankton do also, since $(N_1^*, P_1^*, 0)$ is never stable but $(N_0, 0, 0)$ can be. This can be seen by writing (3) as

$$\frac{\mathrm{d}Z}{\mathrm{d}t} = \left(\frac{\alpha\lambda P^2}{\mu^2 + P^2} - dZ^{m-1} \right) Z \tag{9}$$

and noting that the first term in the brackets is positive as long as $P > 0$, and so as Z gets small, the bracketed term will at some stage become positive, meaning that $\mathrm{d}Z/\mathrm{d}t > 0$, and so Z will increase. The strictly positive growth of the zooplankton will always outweigh the mortality when Z is sufficiently small.

Now consider steady states of the form (N^*, P^*, Z^*) with $N^*, P^*, Z^* > 0$. For $m > 1$, $\mathrm{d}Z/\mathrm{d}t = 0$ gives

$$Z = \left(\frac{\alpha\lambda P^2}{d(\mu^2 + P^2)} \right)^{\frac{1}{m-1}}, \tag{10}$$

which can be substituted into $\mathrm{d}N/\mathrm{d}t = 0$ and $\mathrm{d}P/\mathrm{d}t = 0$ to give two simultaneous equations for N and P, but these cannot be solved analytically to give steady-state values N^* and P^*. Numerical experiments indicate that the stability properties for $1 < m < 2$ are the same as for $m = 2$. Thus the two transcritical bifurcations for $m = 1$ are a special case – for $1 < m \leqslant 2$ the three-way transcritical bifurcation is generic, and the bifurcation diagram is qualitatively similar to Fig. 3.

5. Hopf bifurcations

It is known that for both $m = 1$ and $m = 2$, two Hopf bifurcations occur as d is varied with all of the other parameters fixed at their default values [12,13]. In Fig. 4 we start from $m = 1$, and trace each Hopf bifurcation as m increases, allowing d to vary but keeping all other parameters fixed. The Hopf bifurcations can be traced continuously as m increases from 1, and so $m = 1$ is not a special case for these bifurcations, unlike the transcritical bifurcations calculated above. As m increases further, it is seen that the Hopf bifurcations persist, reaching $m = 2$ at the known values of d for Hopf bifurcations given in [12]. Thus the Hopf bifurcations at $m = 1$ and $m = 2$ are the 'same' Hopf bifurcations, and there is nothing degenerate about any particular value of m. The region of oscillatory behaviour bounded by the Hopf bifurcations thus also persists across the range of m.

6. Persistence of chaos

A chaotic attractor, resulting from a sequence of period-doubling bifurcations, is known to exist for $m = 1$, when $d = 0.142$ and $N_0 = 1.0$, with all other parameters set to their default values [13]. However, for $m = 2$, no period-doubling bifurcations were found as N_0 and d were varied [12]. Thus, we now investigate the existence of chaos as m is varied.
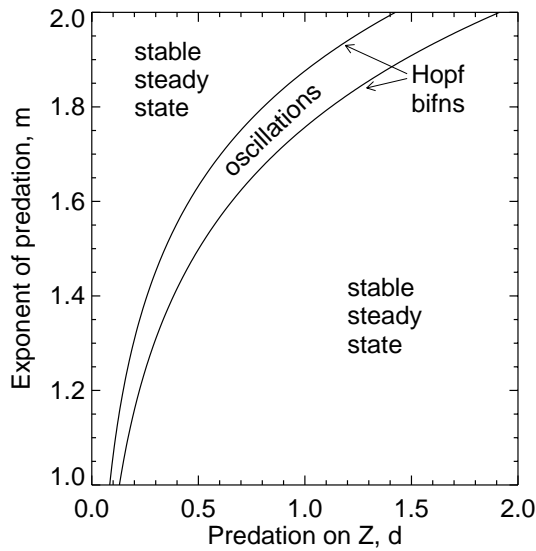
Fig. 4. Location of Hopf bifurcations as m and d vary, showing how the bifurcations persist as m goes from 1 to 2. Unlike the transcritical bifurcations, the Hopf bifurcations exist continuously as m reaches 1. Units of d are (g C m^{-3})$^{1-m}$ day^{-1}, and m is dimensionless.
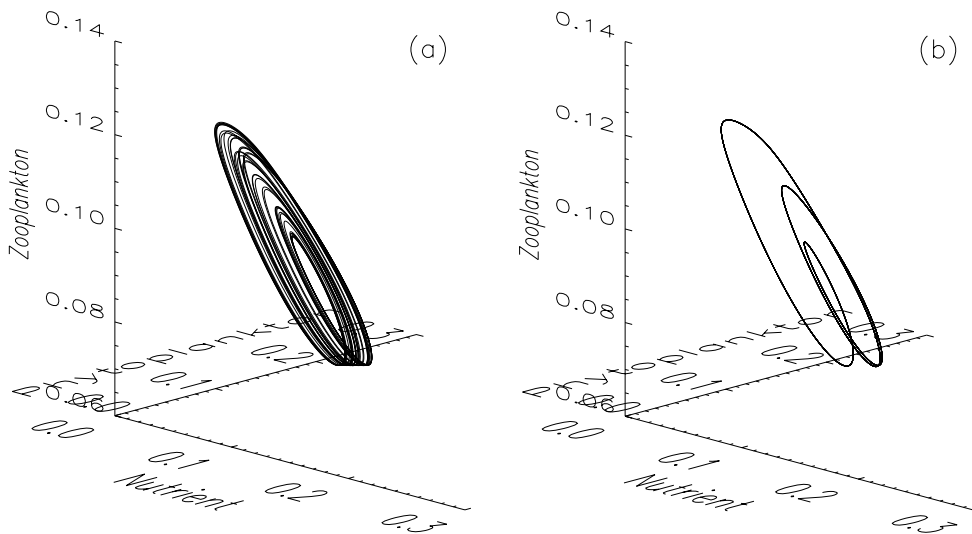

Fig. 5. (a) Chaotic attractor for $m = 2$, starting from the initial conditions $(N, P, Z) = (0.3, 0.1, 0.05)$, in units of g C m^{-3}, with parameter values $a = 0.25$, $b = 0.2$, $c = 0.5$, $d = 0.5$, $e = 0.02$, $k = 0.01$, $r = 0.15$, $s = 0.05$, $N_0 = 1.02$, $\alpha = 0.2$, $\beta = 0.6$, $\gamma = 0.5$, $\lambda = 0.3972$ and $\mu = 0.02$. The transient behaviour is not shown. (b) Starting from the alternative initial conditions $(N, P, Z) = (0.4, 0.1, 0.05)$ a simple cycle is reached.

Firstly, we have found a chaotic attractor for $m = 1.01$, $d = 0.1453$ and $N_0 = 1.0$ (i.e., close to the known chaotic attractor for $m = 1$), which arises from a sequence of period-doubling bifurcations. So we know that chaos is not an artifact of $m = 1$ in this model, unlike the two transcritical bifurcations analysed earlier.

Moreover, in Fig. 5(a) we show a chaotic attractor for the particular case of $m = 2$ (the remaining parameter values are given in the caption). Notice that the attractor does not exhibit the 'tea-cup' shape of the Hastings and Powell attractor [17]. Caswell and Neubert [16] presented chaotic attractors for the Hastings and Powell model with varying closure terms, and the tea-cup shape was retained for quadratic

closure. The attractor in Fig. 5(a) actually coexists with the period-three cycle shown in Fig. 5(b), which is reached from alternative initial conditions (for clarity, the transients are not shown). Each loop of both the chaotic and period-three cycles has a period of about 45 days. Further searches of parameter space reveal other regions of chaotic behaviour, potentially disconnected, where two coexisting attractors are found.

7. Discussion

We have investigated the bifurcational structure of a simple plankton model with a non-integer exponent of closure. Closure terms are used in models to represent predation on zooplankton when the predator population itself is not being explicitly simulated as a separate variable. Closure terms are usually linear or quadratic – the non-integer formulation allows feeding strategies intermediate between those assumed by the linear and quadratic forms. The predators may adopt different feeding strategies depending upon the local turbulent conditions of the water.

We have established which aspects of dynamical behaviour are generic to either the linear or the quadratic closure. We found that the three-way transcritical bifurcation of the steady states is the generic case, with linear closure ($m = 1$) being the only exception, yielding two separate transcritical bifurcations. An alternative closure term that is occasionally used is $qZ + dZ^2$, where q is the linear rate and d the quadratic rate, e.g. [16,24]. This closure term has previously been found to exhibit the two separate transcritical bifurcations [13], suggesting that the linear case is the generic case, and showing that the three-way transcritical bifurcation is structurally unstable. So here we were surprised (at first) to find the quadratic case to be the generic case when dZ^m is used. This emphasises that the meaning of generic can only be referred to the particular form of closure being considered, namely dZ^m in this paper.

The Hopf bifurcations previously identified for linear and quadratic closure were found to stem from the same dynamical mechanism, as found by using the non-integer exponent, m. Chaotic attractors, although occurring for small windows of parameter space, also appear to occur for all m. Thus although the steady-state behaviour is unique at $m = 1$, limit cycles and chaotic dynamics have no special characteristics at $m = 1$.

Recent interest in the influence of the choice of closure term, e.g. [16,25,26], stems from findings [4] (re-examined by [27]) that limit cycles were eliminated from a model's results when quadratic replaced linear closure. It had been thought that this may be a general result, and, by implication, also apply to the existence of chaotic attractors. Here we have shown explicitly how cycles can persist as the closure is smoothly varied from linear to quadratic, and that chaos can occur for the quadratic closure term. Complementing the work of [16], our results further demonstrate that quadratic closure does not preclude the existence of cycles or chaos.

References

[1] Steele JH, Henderson EW. A simple plankton model. Am Nat 1981;117:676–91.
[2] Evans GT, Parslow JS. A model of annual plankton cycles. Biol Oceanogr 1985;3:327–47.
[3] Franks PJS, Wroblewski JS, Flierl GR. Behavior of a simple plankton model with food-level acclimation by herbivores. Mar Biol 1986;91:121–9.
[4] Steele JH, Henderson EW. The role of predation in plankton models. J Plankton Res 1992;14:157–72.
[5] Wroblewski JS. A model of the spring bloom in the North Atlantic and its impact on ocean optics. Limnol Oceanogr 1989;34:1563–71.
[6] Fasham MJR, Ducklow HW, McKelvie SM. A nitrogen-based model of plankton dynamics in the oceanic mixed layer. J Mar Res 1990;48:591–639.

[7] Denman KL, Gargett AE. Biological–physical interactions in the upper ocean: the role of vertical and small scale transport processes. Annu Rev Fluid Mech 1995;27:225–55.

[8] Fasham MJR. Variations in the seasonal cycle of biological production in subarctic oceans: a model sensitivity analysis. Deep-Sea Res I 1995;42:1111–49.

[9] Marrasé C, Costello JH, Granata T, Rudi Strickler J. Grazing in a turbulent environment: energy dissipation encounter rates, and efficacy of feeding currents in *Centropages hamatus*. Proc Natl Acad Sci USA 1990;87:1653–57.

[10] Thomas WH, Gibson CH. Effects of small-scale turbulence on the dinoflagellate, *Gymnodinium sanguineum (splendens)*: contrasts with *Gonyaulax (Ligulodinium) polyedra*, and the fishery implication. Deep-Sea Res 1992;39:1429–37.

[11] Saiz E, Kiørboe T. Predatory and suspension feeding of the copepod *Arcatia tonsa* in turbulent environments. Mar Ecol Prog Ser 1995;122:147–58.

[12] Edwards AM, Brindley J. Oscillatory behaviour in a three-component plankton population model. Dyn Stab Syst 1996;11:347–70.

[13] Edwards AM, Brindley J. Zooplankton mortality and the dynamical behaviour of plankton population models. Bull Math Biol 1999;61:303–39.

[14] Ryabchenko VA, Fasham MJR, Kagan BA, Popova EE. What causes short-term oscillations in ecosystem models of the ocean mixed layer? J Mar Syst 1997;13:33–50.

[15] Huisman J, Weissing FJ. Biodiversity of plankton by species oscillations and chaos. Nature 1999;402:407–10.

[16] Caswell H, Neubert MG. Chaos and closure terms in plankton food chain models. J Plankton Res 1998;20:1837–45.

[17] Hastings A, Powell T. Chaos in a three-species food chain. Ecology 1991;72:896–903.

[18] Edwards AM. A rational dynamical-systems approach to plankton population modelling, PhD Thesis. University of Leeds, UK, 1997.

[19] Platt T, Sathyendranath S, Ravindran P. Primary production by phytoplankton: analytic solutions for daily rates per unit area of water surface. Proc R Soc Lond, Ser B 1990;241:101–11.

[20] Platt T, Sathyendranath S. Estimators of primary production for interpretation of remotely sensed data on ocean color. J Geophys Res 1993;98:14561–76.

[21] Truscott JE. Temporal and spatial behaviour of plankton ecosystems. PhD Thesis, University of Leeds, UK, 1994.

[22] Khibnik AI, Kuznetsov YA, Levitin VV, Nikolaev EV. Interactive LOCal BIFurcation Analyzer. Computer Algebra Netherlands, 1992.

[23] Khibnik AI, Kuznetsov YA, Levitin VV, Nikolaev EV. Continuation techniques and interactive software for bifurcation analysis of ODEs and iterated maps. Physica D 1993;62:360–71.

[24] McGillicuddy DJ, McCarthy JJ, Robinson AR. Coupled physical and biological modeling of the spring bloom in the North Atlantic (I): model formulation and one dimensional bloom process. Deep-Sea Res I 1995;42:1313–57.

[25] Pitchford J, Brindley J. Intratrophic predation in simple predator–prey models. Bull Math Biol 1998;60:937–53.

[26] Sharada MK, Yajnik KS. Effect of nonlinear mortality and self-grazing on the dynamics of a marine ecosystem. Sādhanā 1999;24:17–24.

[27] Edwards AM, Yool A. The role of higher predation in plankton population models. J Plankton Res 2000 (in press).